AIP Journal of Applied Physics

Effect of thickness on dielectric, ferroelectric, and optical properties of Ni substituted Pb(Zr0.2Ti0.8)O3 thin films

Shalini Kumari, Nora Ortega, Dhiren K. Pradhan, Ashok Kumar, J. F. Scott, and Ram S. Katiyar

Citation: Journal of Applied Physics **118**, 184103 (2015); doi: 10.1063/1.4935481
View online: http://dx.doi.org/10.1063/1.4935481
View Table of Contents: http://scitation.aip.org/content/aip/journal/jap/118/18?ver=pdfcov
Published by the AIP Publishing

Effect of thickness on dielectric, ferroelectric, and optical properties of Ni substituted $Pb(Zr_{0.2}Ti_{0.8})O_3$ thin films

Shalini Kumari,[1,a)] Nora Ortega,[1] Dhiren K. Pradhan,[1] Ashok Kumar,[2] J. F. Scott,[3] and Ram S. Katiyar[1,a)]
[1]*Department of Physics and Institute for Functional Nanomaterials, University of Puerto Rico, San Juan, Puerto Rico 00931-3334, USA*
[2]*National Physical Laboratory (CSIR), Delhi, India*
[3]*Department of Chemistry and Department of Physics, University of St. Andrews, St. Andrews KY16 ST, United Kingdom*

(Received 30 June 2015; accepted 28 October 2015; published online 13 November 2015)

We report thickness dependent dielectric, ferroelectric, and optical properties of Ni substituted $Pb(Zr_{0.2}Ti_{0.8})O_3$ thin films. The $Pb(Zr_{0.2}Ti_{0.8})_{0.70}Ni_{0.30}O_{3-\delta}$ (PZTNi30) thin films for various thicknesses, ranging from 5 nm to 400 nm, were fabricated by pulsed laser deposition technique. Giant dielectric dispersion, low dielectric loss, large dielectric constant ~1000–1500 from 100 Hz to 100 kHz, and diffused dielectric anomaly near 570–630 K were observed in PZTNi30 thin films. These films show well saturated ferroelectric hysteresis, with large remanent polarization. It also illustrated excellent optical transparency which decreased from 82 to 72% with increasing film thickness from 5 nm to 400 nm for the probe wavelengths ranging from 200 to 1100 nm. A decrease in direct bandgap (E_g) values from 4 eV to 3.4 eV and indirect-E_g values from 3.5 eV to 2.9 eV were observed for PZTNi30 thin films with increase in film thickness from 5 nm to 400 nm, respectively. The direct and indirect bandgaps were discussed in context of film thickness and grain size effects. Our investigations on optical properties of PZTNi30 thin films suggest that bandgap can be modified as a function of film thickness which may be useful for readers working to develop novel candidates for ferroelectric photovoltaic. © *2015 AIP Publishing LLC*.
[http://dx.doi.org/10.1063/1.4935481]

I. INTRODUCTION

Ferroelectric (FE) materials have recently attracted extensive attention as promising candidates for use in photovoltaic devices and for coupling of light with other functional properties.[1–4] The immense interest in optically active FE materials is due to the presence of strong spontaneous polarization which is necessary for ferroelectric photovoltaic currents, and control of photocurrents using the polarization direction.[5,6] Breaking of inversion symmetry in FE materials develops desirable separation of photo-excited charge carriers and produces photo-voltage higher than the bandgap.[1,3] Generally, metal/ferroelectric/metal device structures not only produce the photo-excited electron-hole pairs but also provide a polarization-induced internal electric field to separate the charge carriers.[3] In order to integrate ferroelectrics into suitable nanoscale devices, miniaturization is often necessary. With the continued quest for ferroelectric photovoltaic (PV) applications, it is becoming increasingly important to scale the dimension of ferroelectrics down to the nanometer-scale size and thorough understanding of miniaturization effects on the material properties. In general, ferroelectric materials are wide band gap insulators with low leakage currents.[1,3,7] The open circuit voltage (V_{oc}) of solar cell is typically limited by the bandgap of the material; hence, the tailoring of band gap of ferroelectric materials with doping of transition metal ions at B-site is a long-standing challenge.[4] Theoretically, it has been proposed that metallic defects, substitutions of transition metal ions can reduce the band gap of ferroelectric materials, which is a basic requirement for their applications as photovoltaic devices for complete solar spectrum.[8–10]

The polarization of FE materials can also be tuned via strain-polarization coupling. Stained ferroelectric films exhibit polarization and dielectric values superior to the corresponding bulk counterpart. Various methods have been employed to develop strain in ferroelectric materials, such as by growing films on large lattice mismatched substrates, homogeneous distribution of defects/vacancies, and by doping of suitable ions into the bulk material. Depending on the substrate-film mismatch combination, either compressive or tensile strains can be introduced. These strains are capable to tilt the polarization vector from out-of-plane to in-plane.[11–13] Nanoscale FE films have shown considerable strain, either due to external strain via lattice mismatch or internal strain due to misfit dislocations/defects.

Recently, photovoltaic properties were observed in many perovskite ferroelectric materials, such as $Pb(Zr_xTi_{1-x})O_3$ (PZT), $BaTiO_3$, $LiNbO_3$, $BiFeO_3$, $(KNbO_3)_{1-x}(BaNi_{1/2}Nb_{1/2}O_{3-\delta})_x$(KBNNO), and PLZT.[1–3,14–16] Yang *et al.*[2] have shown that photovoltaic effect in $BiFeO_3$ (BFO) thin films which have relatively small band gaps (E_g ~2.6–2.9 eV) arises from a unique mechanism, namely, structurally driven steps of the electrostatic potential at nanometer-scale in-plane domains and domain

[a)]Author to whom correspondence to be addressed. Electronic mail: rkatiyar@hpcf.upr.edu (Ram S. Katiyar), shalinikumari1990@gmail.com (Shalini Kumari).

walls. Thickness dependent photo induced currents were investigated by Qin *et al.*[15] in ferroelectric $Pb_{0.97}La_{0.03}Zr_{0.52}Ti_{0.48}O_3$ under the illumination of ultraviolet light; they observed that photocurrent increases exponentially with the decrease of film thickness. Recently, Grinberg *et al.*[1] have observed enormous potential in solid-solution of potassium-niobate and barium-nickel-niobate perovskite ferroelectrics for photovoltaic (PV) applications with reduced band gap and moderate quantum efficiency.

To enhance photovoltaic properties by bandgap engineering, various theoretical and experimental works are underway by different research groups. Gou *et al.*[8] published theoretical work on $Pb(M_xTi_{1-x})O_{3-x}$ perovskite solid solutions (M = Ni, Pd and Pt) and observed a decrease in band gap by substituting the Ti (B-site) with an O-vacancy-stabilized d^8 M^{2+} cation in this system, which suggests a method for designing highly polar semiconducting oxides for photovoltaic applications. Bennett *et al.*[9,10] have theoretically predicted that partial substitution of different transition metal cations in $PbTiO_3$ (PTO) and $Ba(Ti_{1-x}Ce_x)O_3$ (BTCO) can lower the band gap below 1 eV. Zhou *et al.*[17] investigated the temperature variation of optical properties of ZnO thin films; they observed a decrease in band gap with increase of thickness, and they attributed this effect to the change in the stress induced by substrate in the ZnO layer. Pintilie *et al.*[7] found an increase in band gap from 3.9 to 4.4 eV with increase of Zr content in Pb $(Zr_{0.20}Ti_{0.80})O_3$.

In what follows, we have systematically studied structural, dielectric, ferroelectric, and optical properties of Ni-substituted PZT in order to understand its functional properties.[18] The bandgap of $Pb(Zr_{0.2}Ti_{0.8})_{0.70}Ni_{0.30}O_3$-$\delta$ (PZTNi30) thin films also has been established as a function of thickness.

II. EXPERIMENTAL DETAILS

$Pb(Zr_{0.2}Ti_{0.8})_{0.70}Ni_{0.30}O_{3-\delta}$ (PZTNi30) thin films with bottom layer of ITO or $La_{0.67}Sr_{0.33}MnO_3$ (LSMO) were grown by pulsed laser deposition technique on glass or LAO(100) oriented substrates, respectively, employing an excimer laser (KrF, $\lambda = 248$ nm). A schematic diagram of thin film structure is shown in Fig. 1(a). The PZTNi30 and LSMO were grown at 600 °C under an oxygen pressure of 80 mTorr using a laser density of ~3 J/cm^2 and deposition frequency of 5 Hz. After deposition, the as-grown films were annealed in pure oxygen of 300 Torr for 30 min at 700 °C and then cooled down to room temperature slowly. Similar conditions were employed for the thin films grown on ITO coated glass for the optical measurements.

The orientation and phase purity of these films were investigated at room temperature by X-ray diffraction (XRD) using CuK_α radiation with wavelength of $\lambda = 1.5405$ Å. The elemental analysis of fabricated thin films was carried out by high resolution X-ray photoemission spectroscopy (XPS). Atomic force microscopy (AFM-Veeco) was used to examine surface morphology and surface roughness of these films in contact mode. Single frequency excitation piezo force microscopy (PFM) measurements were carried out with a Multimode Nanoscope (Veeco Instruments) in ambient conditions. The conductive tips were used from Bruker coated with

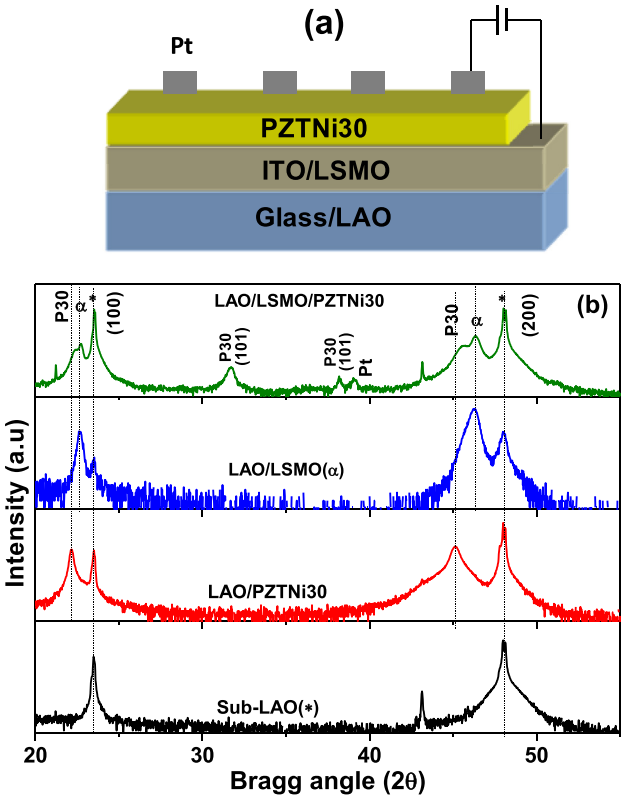

FIG. 1. (a) Schematic diagram of PZTNi30 thin films with bottom layer LSMO/ITO on LAO/glass substrate, (b). Room temperature X-ray diffraction patterns of LAO substrate, PZTNi30 film coated LAO substrate, LSMO film coated LAO substrate, and LAO/LSMO/PZTNi30 thin-film structures.

Pt/Ir. The driving voltage was applied on the surface of the thin film. The resonance frequency of the material is found to be ~360 kHz. The thicknesses of all films were measured using an XP-200 profilometer and filmetrics (F20). To investigate electrical properties, Pt square capacitors were fabricated by dc sputtering as top electrodes with an area of $\sim 10^{-4}$ cm^2 utilizing a metal shadow mask. Frequency dependent dielectric and ferroelectric properties were measured using an HP4294A impedance analyzer and Radiant tester, respectively. Dielectric properties at different temperatures were measured using a MMR Technologies K-20 programmable temperature controller. In order to investigate optical properties of PZTNi30 films with different thickness deposited on ITO-coated glass, transmittance measurements were carried out via UV Visible spectrometer Lambda 2S.

III. RESULTS AND DISCUSSION

A. Structural and elemental characterizations

Fig. 1(b) shows the X-ray diffraction (XRD) patterns of highly oriented PZTNi30 thin films of thickness 400 nm grown on LSMO/LAO (100) substrate recorded at room temperature (top). For comparison, the XRD patterns of LAO substrate (*), PZTNi30 (P30) on LAO substrate, and LSMO (α) on LAO substrate were also included in Fig. 1(b). The θ-2θ scan suggests highly oriented films in the range 20°–60°, which consists of two major diffraction peaks that can be assigned to (100), (200) perovskite PZTNi30, LSMO, and single crystal LAO [both PZTNi30 and LSMO are

overlapping, see doted lines in Fig. 1(b)]. Small amounts of PZTNi30 [(101)–6%, and (111)–2% of main peak] and Pt which was used as top electrode were also observed in the diffraction patterns. All these peaks correspond to perovskite phase with tetragonal crystal structure.[19–21] No diffraction peaks from lead-deficient pyrochlore phases were detected in these pattern, indicating phase purity without appearance of any additional peaks or intermediate phase. The shifting of (100) and (200) peaks from 22.34° to 22.17° and 45.37° to 45.13° were seen in PZTNi30 grown on LAO substrate compared to PZTNi30 grown on LSMO/LAO. The slight shift of XRD pattern towards lower angles indicates a tensile strain of ~0.2% along the LSMO/film interface. The strain (ε) in these films due to lattice mismatch (or misfit) was calculated using the following equation:

$$\mathcal{E} = \frac{a_{substrate} - a_{film}}{a_{substrate}} \times 100, \quad (1)$$

where ε is the lattice strain, $a_{substrate}$ is the lattice constant of the substrate, and a_{film} is the lattice constant of the film.[22] If $\varepsilon > 0$, films will experience in-plane tensile strain and out-of-plane compressive strain, and $\varepsilon < 0$ films will experience in-plane compressive strain and out-of-plane tensile strain near the film-substrate interface. However, with increasing film thickness, film lattices relax to the original bulk lattice constants. Bulk LAO has a pseudocubic unit cell with a = 3.790 Å, while bulk LSMO has a rhombohedral crystal structure with lattice parameter a = 3.871 Å.[23,24] We have already reported in our previous work that the PZTNi30 bulk shows a tetragonal structure with lattice constants a = 3.9639 Å, c = 4.1279 Å, and tetragonality ratio (c/a) 1.041.[18] It was found that PZTNi30 on LAO and PZTNi30 on LAO/LSMO films experience in-plane compressive strain of −4.59% and −2.40%, respectively, near the interface.

To confirm the existence of Ni and its possible oxidation states, high-resolution X-ray Photoelectron spectroscopy (XPS) measurements have been carried out on PZTNi30 films of thickness 400 nm; the corresponding spectra are shown in Fig. 2. The characteristic peaks of Pb $4f_{7/2}$(137.55 eV), Pb $4f_{5/2}$ (142.37), Zr $3d_{5/2}$(180.94), Zr $3d_{3/2}$(183.19), Ti $2p_{3/2}$(457.39), Ti $2p_{1/2}$(463.1), Ni $2p_{3/2}$(854.70), Ni $2p_{1/2}$(872.82), and O 1s (530.34) were observed, as shown in Fig. 2(a). The systematic shifts of the spectra were corrected with the help of the carbon 1S (284.6 eV) line. Fig. 2(b) shows XPS experimental spectrum (open circle), fitted data (pink solid line), and Shirley-type background (orange solid circle) for Ni$2p_{3/2}$, and its inset shows the Ni 2p signals at binding positions of 854.70 eV (Ni $2p_{3/2}$) and 872.82 eV (Ni $2p_{1/2}$) along with their associated satellite peaks of ~879.09 eV (Ni $2p_{1/2}$) and ~861.03 eV (Ni $2p_{3/2}$). The observed binding energy positions of Ni 2p have been observed to be shifted slightly towards higher binding energies; this might be due to a decrease of electron charge density on the ions.[25] The observed binding energy difference between Ni 2p doublet spectra, i.e., $2p_{3/2}$ and $2p_{1/2}$, is found to be ~18.12 eV, whereas the standard doublet separation is ~18.4 eV for NiO and ~17.4 eV for metallic Ni.[26] Thus, it seems that

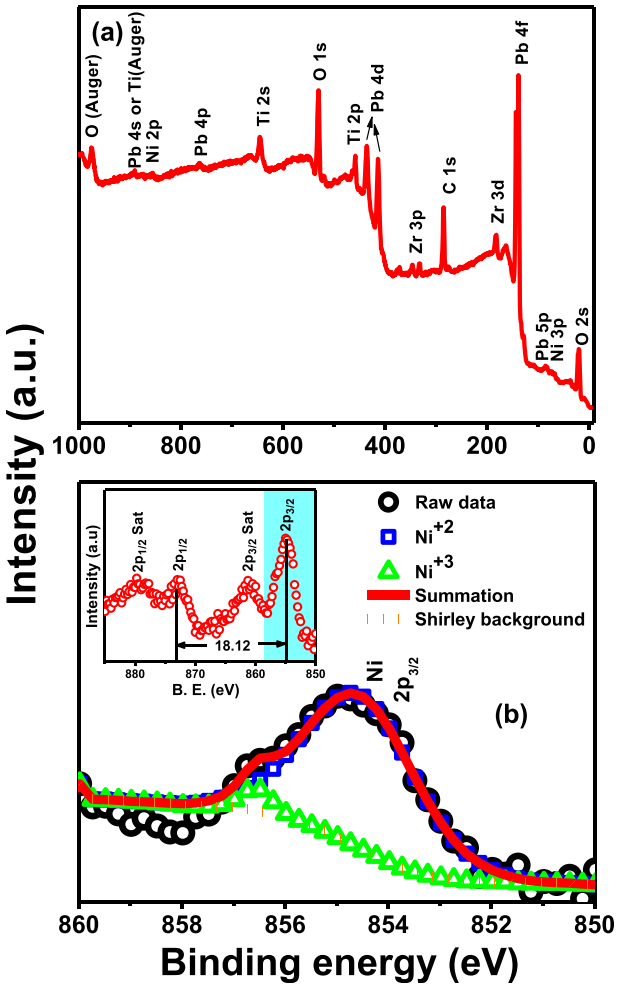

FIG. 2. Detailed XPS scan: (a) full spectra, (b) deconvolution of Ni $2p_{3/2}$ peak; inset shows a full spectrum of Nickel in LAO/LSMO/PZTNi30 thin film of thickness 400 nm at room temperature.

there is a clear presence of Ni-O bonding with possible occupation of Ni at the center of BO_6 octahedral. The Ni $2p_{3/2}$ spectra have been deconvoluted into two clear peaks, which is due to the mixed valence states of Ni (+2 and +3). The deconvoluted area ratio of Ni^{+2} and Ni^{+3} was found to be 96:4 from the Ni $2p_{3/2}$ peak. Hence, metastable states of Ni^{+2}/Ni^{+3} ions were confirmed through XPS measurement.

B. Electrical characterization

In order to confirm the existence of ferroelectricity at nano-scale, the fabricated PZTNi30 films of thickness ~400 nm were characterized by piezo response force microscopy at randomly selected areas. Fig. 3 shows a phase image of a LAO/LSMO/PZTNi30 film obtained after poling 4×4 μm^2 area by +9 V and then the central 2×2 μm^2 area was poled by −9 V bias. Three types of polarization states were observed: as-grown unpoled outside area, positively biased area (+9 V), and at the center a negative-biased area (−9 V). The brown region indicates the area that was poled with positive bias, and the white region indicates the area that was poled with negative electric field. A random polarization orientation was found in as-grown films, whereas polarizations could be switched easily with positive and negative bias.

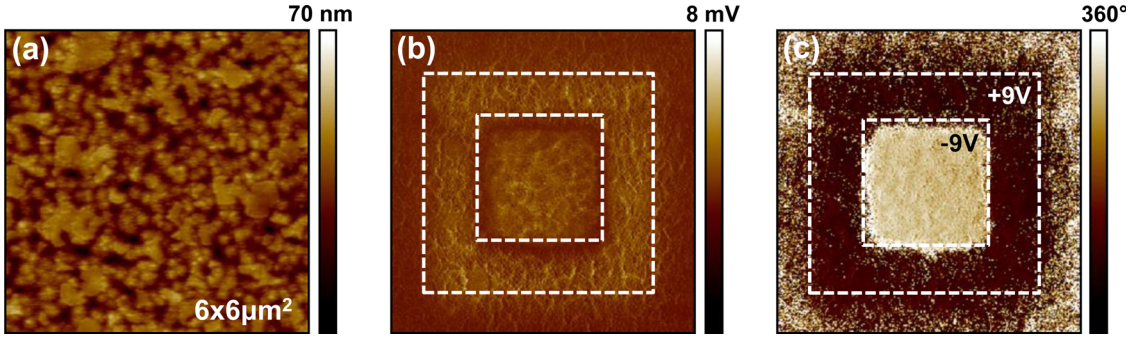

FIG. 3. Piezo force microscopy: (a) Topographic (6 μm × 6 μm), (b) amplitude, and (c) phase image of LAO/LSMO/PZTNi30 thin film of thickness 400 nm.

The frequency dependence of relative dielectric permittivity (ε_r) and loss tangent ($\tan\delta$) of PZTNi30 thin films with different thicknesses at room temperature are shown in Fig. 4(a). The measurements were done with an oscillation level of 100 mV. Fig. 4(a) shows that the dielectric constant ε_r and the loss $\tan\delta$ increase from 200 to 1000 and 0.05 to 0.11, respectively, at 1 kHz when thickness of films increases from 100 to 400 nm. The decrease in dielectric constant with decrease of film thickness can be explained on the basis of extrinsic and intrinsic contributions to the dielectric properties in ferroelectric thin films.[27–29] The ε_r for all films is stable over a wide range of frequency $<10^5$ Hz and shows strong frequency dispersion with a substantial decrease above 10^5 Hz. The loss tangent is almost constant, <0.10, in the frequency range 10^2 to 10^4 Hz; above 10^4 Hz, a drastic increase was observed in loss tangent with increase of frequency. At high-frequency low dielectric constant and high loss may be due to semiconducting nature of the bottom electrode and its response to the probe frequency.[30] An improvement in dielectric constant was observed for Ni-substituted PZT thin films compared to pure PZT.[31,32] The observed enhancement in dielectric constant may be due to the existence of large grains seen in surface morphology (micrograph shown in Fig. 3(a)).[33]

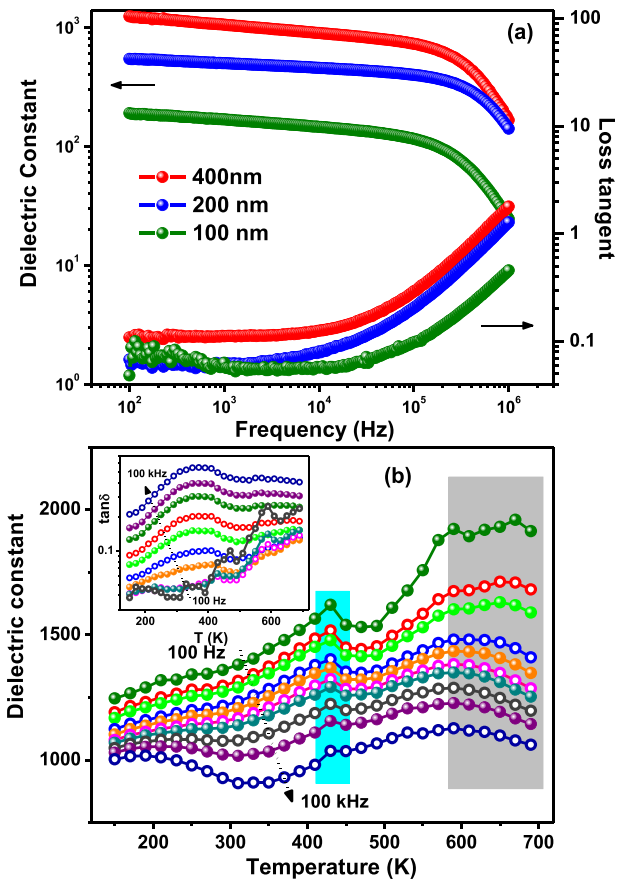

FIG. 4. (a) Frequency dependent dielectric constant (ε_r) and loss tangent ($\tan\delta$) of LAO/LSMO/PZTNi30 thin films of different thickness at room temperature; (b) temperature dependent ε_r and $\tan\delta$ (inset) of LAO/LSMO/PZTNi30 thin films of thickness 400 nm at different frequencies.

Relative permittivity as a function of temperature is the most common tool to observe phase transitions in ferroelectric materials. Fig. 4(b) presents the temperature dependent dielectric permittivity (ε_r) plot of the PZTNi30 films of thickness 400 nm at various frequencies. A decrease in ε_r with increasing frequency is a signature of polar dielectrics. The ε_r increases gradually, exhibiting one sharp and a second broad peak around 430 K and 570–630 K, respectively. We attribute the sharp shoulder around 430 K to the ferromagnetic-paramagnetic phase transition of LSMO; a similar anomaly was observed by Dussan *et al.*[30] at around 400 K for PZT/LSMO heterostructures. This transition is almost frequency-independent. The second shoulder occurs around 570–630 K and is diffuse, which may be due to thermally excited charge carriers. These films do not show any ferroelectric-paraelectric phase transition within experimental limits. The temperature dependence of $\tan\delta$ is depicted in the inset of Fig. 4(b). The loss tangents were observed to be less than ~0.55 in the whole frequency range. Broad peaks around 400 K relates to the ferromagnetic-paramagnetic phase transition of LSMO, and the second sharp peak around 600 K corresponds to thermally activated charge carriers.

The size of top electrodes influences the ferroelectric characteristics, so we have fabricated top electrodes of small area (0.0001 cm^2). The thickness-dependent polarization-electric field (P-E) loops which directly show the ferroelectric behavior of PZTNi30 films at room temperature are depicted in Fig. 5(a). A fundamental parameter of a ferroelectric is the absolute remanent polarization (P_r), which can be measured from the P-E loops by subtracting parasitic contributions such as linear capacitances and leakage currents.[34] Well-saturated P-E loops were observed for PZTNi30 films of different thickness at room temperature, shown in Fig. 5(a). A slight increase in P_r was also observed with increase of thickness.

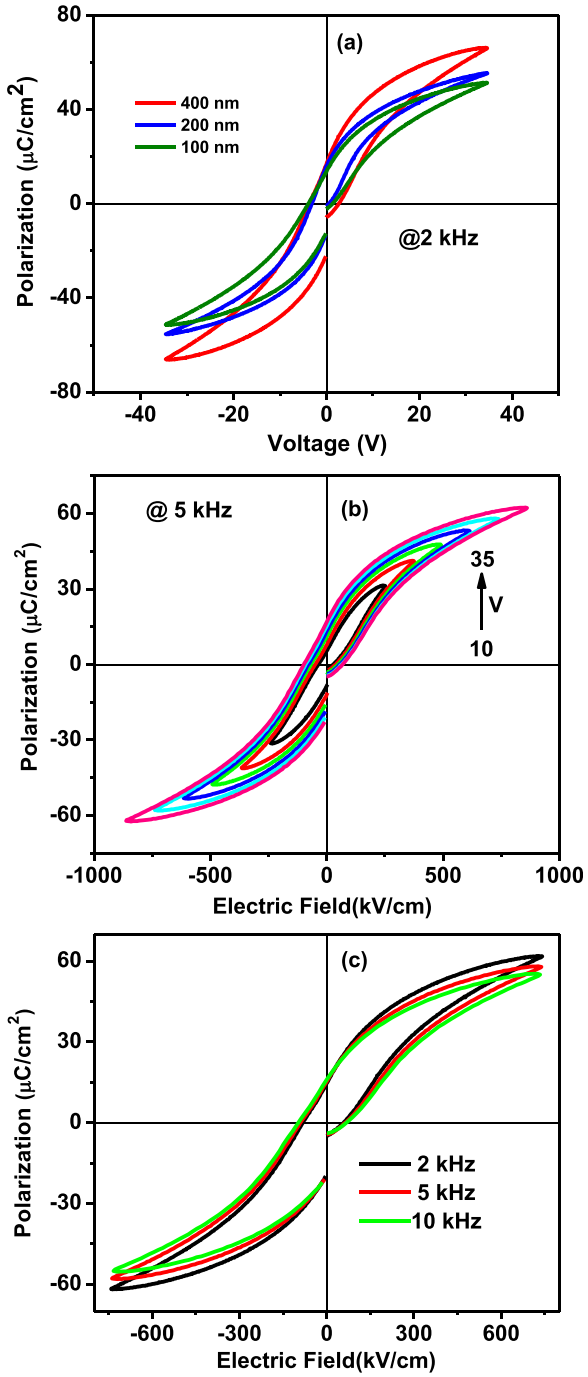

FIG. 5. (a) Thickness dependent ferroelectric loops (P-E loops) at 35 V; (b) P-E loop at 5 kHz at different applied voltages (10–35 V); (c) frequency-dependent P-E loops at 30 V at room temperature.

The values of P_r for the PZTNi30 thin films were found in the range of 13–20 $\mu C/cm^2$ for different PZTNi30 film thickness. Sakashita *et al.*[35] have investigated thickness-dependent electrical properties in PZT thin films and observed gradual decreases in P_r with decrease of film thickness, attributed to intrinsic stress. Figs. 5(b) and 5(c) present the frequency and voltage dependent P-E loops for PZTNi30 films of thickness 400 nm. The P_r and the coercive field (E_c) were found to be $\sim$20 $\mu C/cm^2$ and 75 kV/cm at 5 kHz with maximum applied electric field. From Fig. 5(b), we found gradual enhancement in spontaneous polarization (P_s), P_r, and E_c with an increase of electric field at frequency 5 kHz. There is no significant change in P_r and E_c with increase of frequency, as can be seen in Fig. 5(c). A clear shift in P-E loops was seen towards the negative voltage side, which is due to high in-built electric field. The observed imprint behavior is due to different work functions of dissimilar top and bottom electrodes (Pt and LSMO)[36] or the presence of extra stress at the interface originating during high temperature annealing process.[33] It may also arise from space charge at the ferroelectric/electrode interface.[36]

1. Optical characterization

To further understand the effect of Ni-doping on bandgap of pure PZT, we analyzed the optical properties of PZTNi30 thin films. Transmission spectroscopy is a useful technique to evaluate the bandgap of the as-grown thin films. Fig. 6(a) shows the room temperature optical transmission spectra of the PZTNi30 films on Sn-doped In_2O_3 (ITO)-coated glass for different thickness along with ITO/glass substrate, recorded in the wavelength range 200–1100 nm. In the visible wavelength region (400–800 nm), the films were found highly transparent with a transmittance between 60%–80%; this property is important since for photovoltaic applications transparent PZTNi is needed. The transmittance % for PZTNi30 thin films of different thickness at wavelength 600 nm are tabulated in Table I. From transmission spectra, we can identify two main characteristics: interference patterns and the absorption edge. The oscillations in the transmittance curve for PZTNi30 thin films are due to interference between the air-film and film-substrate interface. Oscillating transmittance spectra were observed for 200 nm and 400 nm films, suggesting that they have a flat surface and a uniform thickness.[37–39] It was also observed that the number of oscillations decreases with decrease of film thickness. Optical absorption edge was observed at wavelength $\sim$300–350 nm (see Fig. 6(b)) for all films and substrate; with increasing film thickness, the absorption edge is shifted towards higher wavelength, as indicated by the arrow in the inset of Fig. 6(b), which indicates a decrease in the bandgap of the films; this result is in agreement with previous reports.[40,41]

Fig. 6(c) shows the refractive index (n) and extinction coefficient (k) of the PZTNi30 thin films with thickness 200 and 400 nm as a function of wavelength. Calculation of n and k was not possible for thinner films ($t < 200$ nm) due to an insufficient number of oscillations in the transmittance spectra. The n and k values of PZTNi30 thin films have been determined from the transmittance spectra by using "envelope method" originally developed by Manifacier *et al.*[42,43] Using this method, the value of n and k for an insulating film on a transparent substrate can be evaluated as summarized below:
For

$$k^2 \ll (n - n_0)^2 \tag{2}$$

and

$$k^2 \ll (n - n_1)^2, \tag{3}$$

where n_0 and n_1 are the refractive index of air and substrate, respectively, the transmittance of the films can be described as

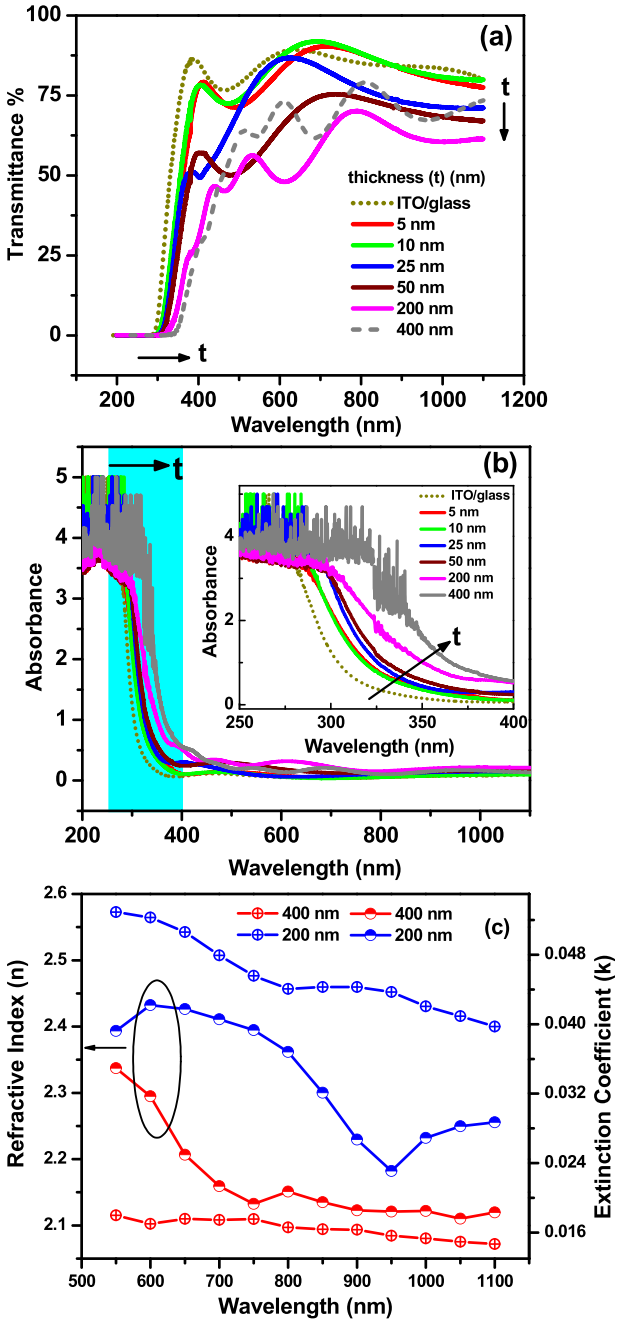

FIG. 6. (a) Thickness dependent Transmittance %; (b) thickness dependent absorbance; (inset) enlarged view of absorbance from wavelength 250 nm to 400 nm for glass/ITO/PZTNi30 thin films between wavelengths 200–1100 nm; (c) refractive index (n) and extinction coefficient (k) vs wavelength of PZTNi30 thin films of thickness 200 and 400 nm.

$$T = \frac{(16n^2 n_0 n_1 \alpha)}{C_1{}^2 + C_2{}^2\alpha^2 + 2C_1C_2\alpha\cos(4\pi nt/\lambda)}, \tag{4}$$

$$\text{Here, } C_1 = (n + n_0)(n_1 + n), \tag{5}$$

$$C_2 = (n - n_0)(n_1 - n), \tag{6}$$

$$n = [N + (N^2 - n_0{}^2 n_1{}^2)^{1/2}]^{1/2}, \tag{7}$$

where

$$N = \frac{n_0{}^2 + n_1{}^2}{2} + 2n_0n_1\frac{T_{\max} - T_{min}}{T_{\max}T_{min}}, \tag{8}$$

TABLE I. Grain size, average (R_a), and root mean square (R_{rms}) surface roughness obtained from atomic force microscopy images and transmittance percentage (T), direct and indirect bandgaps, of PZTNi30 on ITO coated glass substrate for different thickness.

PZTNi 30 film Thickness (nm)	Grain size (nm)	R_a (nm)	R_{rms} (nm)	T (%) at 600 nm	Direct band gap (eV)	Indirect band gap (eV)
400	168	4.02	5.26	72.72	3.4	2.9
200	127	7.04	8.82	56.94	3.6	3.1
100	119	3.98	5.05	…	…	…
50	90	5.73	7.61	64.82	3.8	3.3
25	68	3.22	4.04	86.44	3.9	3.4
10	61	2.65	3.31	86.79	3.95	3.45
5	57	4.14	5.17	82.89	4	3.5
ITO	91	5.66	7.10	88.46	4.1	3.75

$$t = \frac{M\lambda_1\lambda_2}{2(n(\lambda_1)\lambda_2 - n(\lambda_2)\lambda_1)}, \tag{9}$$

and

$$\alpha = \frac{C_1[1 - (T_{max}/T_{\min})^{1/2}]}{C_2[1 + (T_{max}/T_{\min})^{1/2}]}. \tag{10}$$

t and α are the thickness and absorption coefficient of the film, respectively. Thickness of the layer can be calculated using Equation (9), where M = 1 for two consecutive maxima or minima. λ_1, $n(\lambda_1)$ and λ_2, $n(\lambda_2)$ are the corresponding wavelengths and indices of refraction, whereas the value of α can be calculated using Equation (10).

The extreme values of the transmission are given by the formulae

$$T_{max} = \frac{16n_0n_1n^2\alpha}{(C_1 + C_2\alpha)^2}, \tag{11}$$

$$T_{min} = \frac{16n_0n_1n^2\alpha}{(C_1 - C_2\alpha)^2}. \tag{12}$$

After substituting the value of α in the following equation, we can evaluate the value of k:

$$\alpha = \exp\left(-\frac{4\pi kt}{\lambda}\right). \tag{13}$$

In order to calculate these values, the transmittance maximum (T_{max}) and minimum (T_{min}) at a specific wavelength were identified from the envelope in the transmittance spectra of PZTNi30 thin films of thickness 200 and 400 nm shown in Fig. 6(a).[42,43] The calculated values of n were in the range of 2.17–2.43 and 2.11–2.34 for 200 and 400 nm respectively, similar to the values found for PZT thin films.[43–46] The computed values of k were found in the range of 0.04–0.053 and 0.015–0.018 for 200 and 400 nm, respectively, which are comparable with the k value reported earlier for PZT thin films.[43,45,47] The n-values for both films decrease exponentially as the wavelength increases, which is consistent with previously reported behavior of PZT thin films.[43,48,49] However, very slight increase in n at higher wavelength were observed for 200 nm thin films. Higher n-

values were observed for 200 nm compared to 400 nm PZTNi30 thin films, indicating the increase in refractive index with reduction of thickness. Hu *et al.*[48] observed the decreases in refractive index with increasing thickness in the wavelength range 2.5–11 μm for the BST films. Lappalainen *et al.*[49] found that the refractive index varied from 2.28 to 2.46 with the increase of mean grain size for Nd-doped PZT thin films. Increase in refractive index with the reduction of thickness for PZTNi30 thin films can be due to the increase in crystallinity and grain size.[48,49] Monotonic decrease in the k values is seen for both films, especially for 400 nm, with the variation of wavelength matching well with the earlier reported behavior of PZT thin films.[43] The total optical loss caused by absorption and scattering $-k$ values is observed to be low for the PZTNi30 films of thickness 400 nm.

In order to study the effect of thickness on surface morphology of PZTNi30/ITO/glass films and to correlate it with optical properties, atomic force microscopy (AFM) measurements were carried out with regular contact mode over 2 × 2 μm^2 areas for films of different thickness ranging from 5 nm to 400 nm, and ITO/glass substrate, as shown in Fig. 7. The data revealed an evolution in the grain size with the variation of PZTNi30 film thickness, and the main features from AFM images can be summarized as follows: (i) PZTNi30 5-nm films on ITO/glass substrate have small grains compared with the other films; (ii) for 25-nm and 50-nm PZTNi30 films, the small grains start to agglomerate to form large grains; (iii) 100-nm films show clearly a large grain structure embedded with small grains with round shapes (see white arrows in enlarged grain in inset); (iv) 400-nm films present well-defined grain structure with distinct grain boundaries; (v) from Table I, we can see the mean in-plane diameter of the grains increased with film thickness from 57 nm (for t = 5 nm) to 168 nm (for t = 400 nm). Similar microstructures with irregular distribution of grain size were observed for analogous systems like Nb-doped PZT and Ce-doped PZT

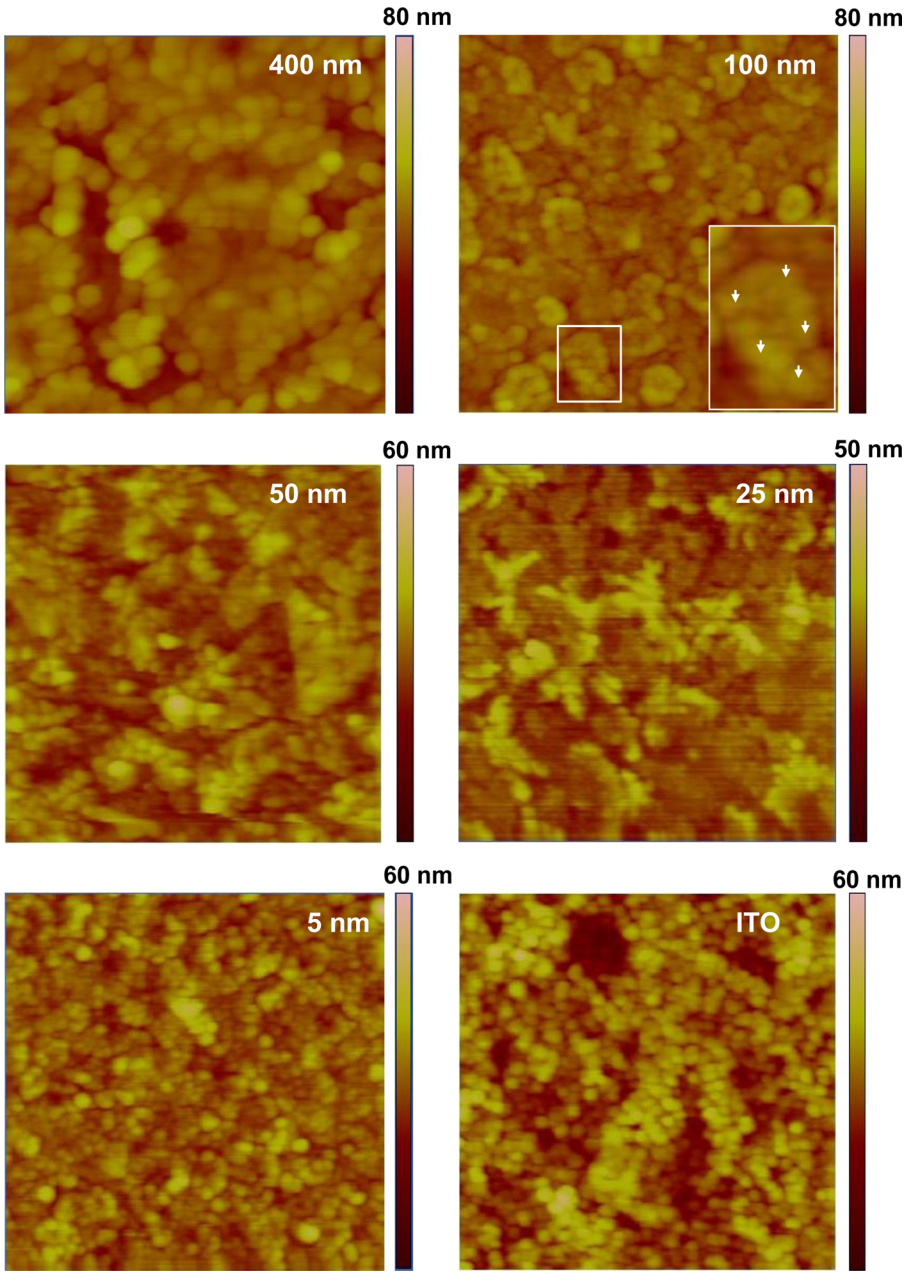

FIG. 7. Thickness dependent atomic force microscopy images of glass/ITO/PZTNi30 thin films.

thin films by Li *et al.*[50] and Majumder *et al.*,[43] respectively. The change in grain size with thickness may be due to (i) small grains coalesce into the larger grains as the thickness of the PZTNi30 increases, and (ii) high stress developed in the film due to the lattice mismatch between film and substrate.

In general, absorption coefficients (α) given in the equation below are related to the photon energy, derived from the Tauc relation[51,52]

$$\alpha h\nu = A(h\nu - E_g)^n, \tag{14}$$

where A is a constant corresponding to electron-hole mobility; h is the Planck constant; ν, the photon frequency; E_g, the band gap; and n, a ratio which characterizes the type of optical transition in the material ($n = 2$, 1/2, 2/3 or 1/3 corresponding to allowed direct, allowed indirect, forbidden direct, and forbidden indirect); and α is calculated using the equation given below

$$\alpha = \left(\frac{1}{d}\right)\ln\left(\frac{1}{T}\right), \tag{15}$$

where d is the thickness of the film and T is its transmittance. Both direct and indirect E_g values for PZTNi30 thin films for different thickness were obtained plotting $(\alpha h\nu)^2$ and $(\alpha h\nu)^{1/2}$ against $h\nu$ as shown in Figs. 8 and 9. E_g values were estimated by extrapolating the linear region in the absorption edge region. The direct band gap was found to be around 3.4 eV for 400 nm PZTNi30 film (less than 3.9 eV of pure $PbZr_{0.2}Ti_{0.8}O_3$) by Ni-substitution at B-site which modified the Ni-O and Ti/Zr-O boding and oxygen vacancies. The most interesting observation is the detection of indirect band gap around ~2.9 eV for same thickness, which may be due to formation of oxygen vacancies and defect levels. Substitution of transition metals at B-site causes the cation octahedral ordering which alters the cation bonding and hence strongly affects the bandgap. The creation of intrinsic oxygen vacancies/defects due to the existence of metastable states of Ni^{+2}/Ni^{+3} may develop the indirect band gap. The presence of impurities, native defects, substitution ions concentrations, and level of structural and thermal disorder might play important role in reducing E_g. The presence of indirect band gap provides high V_{oc} and I_{sc} as it helps to trap different wavelength of solar spectrum. The small direct bandgap tunability and significantly large indirect bandgap tunability open a path towards the classical ferroelectric PZT with transition metal-complex oxides. In this system, introduction of the O vacancy at due B-site of PZT substitution of Ni gives rise to significant distortions of the oxygen lattice and increases all cations' displacement. Substituting the B-site of Pb-based perovskites with transition elements like Ni whose bonds with oxygen are less ionic and more

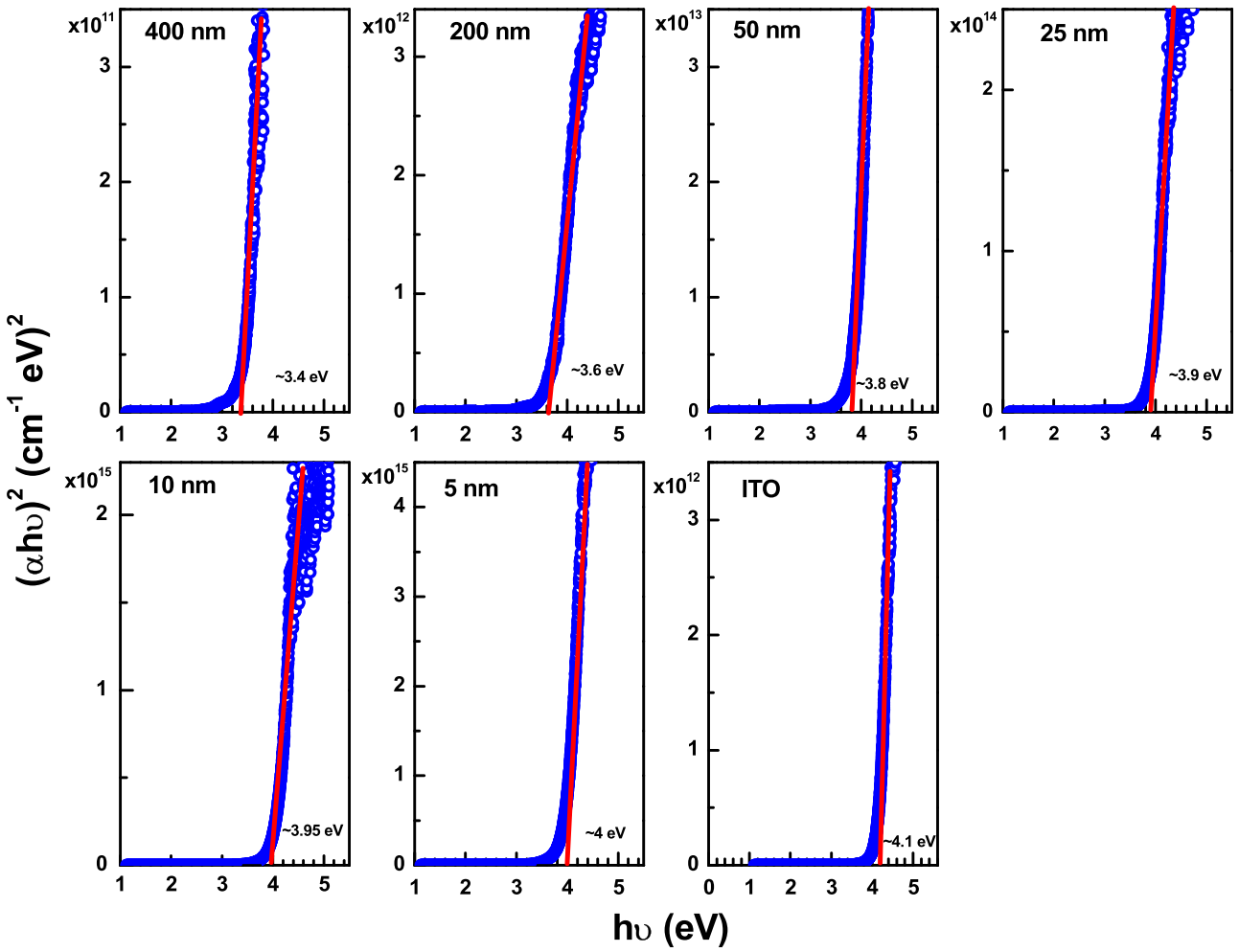

FIG. 8. Thickness dependent direct bandgap of glass/ITO/PZTNi30 thin films.

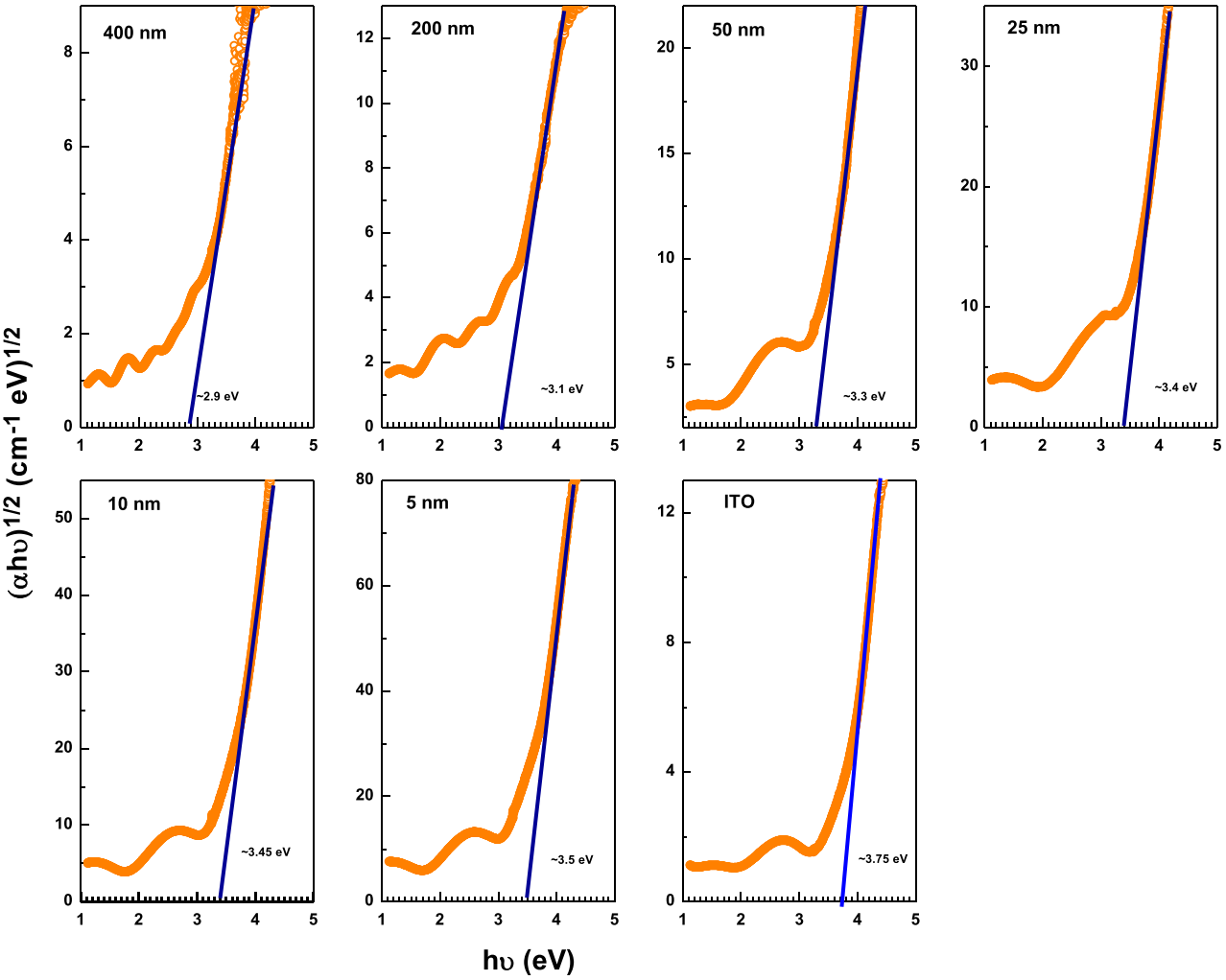

FIG. 9. Thickness dependent indirect bandgap of glass/ITO/PZTNi30 thin films.

covalent due to the complete Ni-O-Ni network and strong hybridization between Ni-d and O-p increases Ni-O bond covalency, resulting smaller E_g.[1,8–10,18] The decrease of band gap by Ni-substitution in different materials has also been reported theoretically and experimentally by other research groups.[8–10,53,54]

Here, the effect of thickness on E_g is our central focus. A decrease was observed in direct-E_g values from 4 eV to 3.4 eV and indirect-E_g values from 3.5 eV to 2.9 eV as the thickness of the films increases from 5 nm to 400 nm. The values of direct/indirect E_g are listed in Table I. The shift of absorption edge towards higher wavelength with increase of thickness reveals a shift of ~0.6 eV for direct and indirect bandgap, respectively. Similar decreases in E_g with increases of film thickness have been observed in Nd modified PZT. They attributed this increase in the E_g value, to quantum size effect in nanocrystalline films, increase of volume ratio of amorphous grain boundaries and defects, or by reduction of the unit cell volume and atomic separation caused by strong residual compressive stress.[41] In another report, similar behavior was observed for $B_{3.25}Nd_{0.85}Ti_3O_{12}$, and it is explained by the quantum-size effect.[40] The increase in band gap with decreasing thickness have been reported in several previous studies.[55,56]

In general, E_g values are very sensitive to: (i) grain size;[57,58] (ii) disorder at the grain boundaries;[59] (iii) lattice parameters-lattice strain;[60,61] (iv) chemical composition;[43] (v) thermal treatment;[41,62,63] (vi) quantum size effect and one-dimensional quantum confinement;[64] and (vii) carrier concentration.[60]

In our case, the increase of E_g with decrease of film thickness can be due to decrease in grain size observed from AFM images (see Fig. 7). The quantum size effect in nanocrystalline films, presence of large grain boundaries/defects and/or by reduced unit cell volume and atomic separation caused by strong residual compressive stress became prominent factors at low dimension systems which significantly modify the optical bandgap. In the present case, it increases with decrease in crystallite size and film thickness.[40,41,51,52,55–64] The other possibility may be the presence of many very small crystallites in these films which may behave like an amorphous phase and may contribute to the absorption spectrum, resulting in higher band gap.[65]

IV. CONCLUSIONS

Crystal structure, surface morphology, and dielectric, ferroelectric, and optical properties of PZTNi30 films were

extensively studied. XPS studies revealed that Ni was present in both +2 and +3 valence states. Systematic correlations have been established among the dielectric, ferroelectric, optical properties, grain size, and film thickness. Significant reduction in direct and indirect bandgap energies are observed with the increase of film thickness. Our investigation on Ni-substituted PZT opens a path for modification of well known ferroelectrics by transition metals for possible ferroelectric photovoltaic and multifunctional applications.

ACKNOWLEDGMENTS

This work was supported by NSF Grant EPS-01002410. N. Ortega acknowledges support from the DoE Grant DE-FG02-08ER46526.

[1]I. Grinberg, D. V. West, M. Torres, G. Gou, D. M. Stein, L. Wu, G. Chen, E. M. Gallo, A. R. Akbashev, P. K. Davies, J. E. Spanier, and A. M. Rappe, Nature **503**, 509 (2013).
[2]S. Y. Yang, J. Seidel, S. J. Byrnes, P. Shafer, C.-H. Yang, M. D. Rossell, P. Yu, Y.-H. Chu, J. F. Scott, J. W. Ager, L. W. Martin, and R. Ramesh, Nat. Nanotechnol. **5**, 143 (2010).
[3]J. Zhang, X. Su, M. Shen, Z. Dai, L. Zhang, X. He, W. Cheng, M. Cao, and G. Zou, Sci. Rep. **3**, 2109 (2013).
[4]R. Guo, L. You, Y. Zhou, Z. S. Lim, X. Zou, L. Chen, R. Ramesh, and J. Wang, Nat. Commun. **4**, 1990 (2013).
[5]H. Lee, Y. S. Kang, S.-J. Cho, B. Xiao, H. Morkoç, T. D. Kang, G. S. Lee, J. Li, S.-H. Wei, P. G. Snyder, and J. T. Evans, J. Appl. Phys. **98**, 094108 (2005).
[6]I. Kanno, H. Kotera, and K. Wasa, Sens. Actuators A **107**, 68 (2003).
[7]L. Pintilie, I. Vrejoiu, G. L. Rhun, and M. Alexe, J. Appl. Phys. **101**, 064109 (2007).
[8]G. Y. Gou, J. W. Bennett, H. Takenaka, and A. M. Rappe, Phys. Rev. B **83**, 205115 (2011).
[9]J. W. Bennett, I. Grinberg, and A. M. Rappe, J. Am. Chem. Soc. **130**, 17409 (2008).
[10]J. W. Bennett, I. Grinberg, P. K. Davies, and A. M. Rappe, Phys. Rev. B **82**, 184106 (2010).
[11]R. Waser and A. Rudiger, Nat. Mater. **3**, 81 (2004).
[12]C.-L. Jia, V. Nagarajan, J.-Q. He, L. Houben, T. Zhao, R. Ramesh, K. Urban, and R. Waser, Nat. Mater. **6**, 64 (2007).
[13]M. J. Polking, M.-G. Han, A. Yourdkhani, V. Petkov, C. F. Kisielowski, V. V. Volkov, Y. Zhu, G. Caruntu, A. P. Alivisatos, and R. Ramesh, Nat. Mater. **11**, 700 (2012).
[14]D. Cao, J. Xu, L. Fang, W. Dong, F. Zheng, and M. Shen, Appl. Phys. Lett. **96**, 192101 (2010).
[15]M. Qin, K. Yao, Y. C. Liang, and S. Shannigrahi, J. Appl. Phys. **101**, 014104 (2007).
[16]R. K. Katiyar, A. Kumar, G. Morell, J. F. Scott, and R. S. Katiyar, Appl. Phys. Lett. **99**, 092906 (2011).
[17]M.-X. Zhou, Z.-W. Li, B. Chen, J.-G. Wan, and J.-M. Liu, J. Phys. D: Appl. Phys. **46**, 165304 (2013).
[18]S. Kumari, N. Ortega, A. Kumar, J. F. Scott, and R. S. Katiyar, AIP Av. **4**, 037101 (2014).
[19]D. Walker, P. A. Thomas, and S. P. Collins, Phys. Status Solidi A **206**, 1799 (2009).
[20]C. Wang, Q. F. Fang, Z. G. Zhu, A. Q. Jiang, S. Y. Wang, B. L. Cheng, and Z. H. Chen, Appl. Phys. Lett. **82**, 2880 (2003).
[21]R. Takayama and Y. Tomita, J. Appl. Phys. **65**, 1666 (1989).
[22]W. Pompe, X. Gong, Z. Suo, and J. S. Speck, J. Appl. Phys. **74**, 6012 (1993).
[23]V. Vonk, M. Huijben, K. J. I. Driessen, P. Tinnemans, A. Brinkman, S. Harkema, and H. Graafsma, Phys. Rev. B **75**, 235417 (2007).
[24]L. J. Belenky, X. Ke, M. Rzchowski, and C. B. Eom, J. Appl. Phys. **97**, 10J107 (2005).
[25]J. S. Corneille, J.-W. He, and D. W. Goodman, Surf. Sci. **306**, 269 (1994).
[26]*Handbook of X-ray Photoelectron Spectroscopy*, by C. D. Wagner, W. M. Riggs, L. E. Davis, J. F. Moulder, and G. E. Muilenberg (Perkin-Elmer Corp., Physical Electronics Division, Eden Prairie, MN, 1979).
[27]T. Haccart, E. Cattan, and D. Remiens, Semicond. Phys. Quantum Electron. Optoelectron. **5**, 78 (2002).
[28]J. Pérez de la Cruz, E. Joanni, P. M. Vilarinho, and A. L. Kholkin, J. Appl. Phys. **108**, 114106 (2010).
[29]D. Barrionuevo, N. Ortega, A. Kumar, R. Chatterjee, J. F. Scott, and R. S. Katiyar, J. Appl. Phys. **114**, 234103 (2013).
[30]S. Dussan, A. Kumar, J. F. Scott, and R. S. Katiyar, Appl. Phys. Lett. **96**, 072904 (2010).
[31]L. Feigl, E. Pippel, L. Pintilie, M. Alexe, and D. Hesse, J. Appl. Phys. **105**, 126103 (2009).
[32]N. Floquet, J. Hector, and P. Gaucher, J. Appl. Phys. **84**, 3815 (1998).
[33]F. Xu, S. T.-McKinstry, W. Ren, B. Xu, Z.-L. Xie, and K. J. Hemker, J. Appl. Phys. **89**, 1336 (2001).
[34]P. M. Leufke, R. Kruk, D. Wang, C. Kübel, and H. Hahn, AIP Adv. **2**, 032184 (2012).
[35]Y. Sakashita, H. Segawa, K. Tominaga, and M. Okada, J. Appl. Phys. **73**, 7857 (1993).
[36]F. Chen, X. Tan, Z. Huang, X. Xuan, and W. Wu, Appl. Phys. Lett. **96**, 262902 (2010).
[37]M. M. Zhu, Z. H. Du, and J. Ma, AIP Adv. **1**, 042144 (2011).
[38]W. Leng, C. Yang, H. Ji, J. Zhang, J. Tang, H. Chen, and L. Gao, J. Phys. D: Appl. Phys. **40**, 1206 (2007).
[39]F. M. Pontes, E. R. Leite, D. S. L. Pontes, E. Longo, E. M. S. Santos, S. Mergulhao, P. S. Pizani, F. Lanciotti, Jr., T. M. Boschi, and J. A. Varela, J. Appl. Phys. **91**, 5972 (2002).
[40]Y. Zang, D. Xie, Y. Chen, M. Li, C. Chen, T. Ren, and D. Plant, J. Sol-Gel Sci. Technol. **61**, 236 (2012).
[41]J. Puustinen, J. Lappalainen, J. Hiltunen, and V. Lantto, Ferroelectrics **370**, 46 (2008).
[42]J. C. Manifacier, J. Gasiot, and J. P. Fillard, J. Phys. E: Sci. Instrum. **9**, 1002 (1976).
[43]S. B. Majumder, Y. N. Mohapatra, and D. C. Agrawal, J. Mater. Sci. **32**, 2141 (1997).
[44]M. P. Moret, M. A. C. Devillers, K. Worhoff, and P. K. Larsen, J. Appl. Phys. **92**, 468 (2002).
[45]G. Teowee, J. M. Boulton, E. K. Franke, S. Motakef, T. P. Alexander, T. J. Bukowski, and D. R. Uhlmann, Integr. Ferroelectr. **15**, 281 (1997).
[46]J. Cardin, D. Leduc, T. Schneider, C. Lupi, D. Averty, and H. W. Gundel, J. Eur. Ceram, Soc. **25**, 2913 (2005).
[47]M. Prabu, I. B. S. Banu, S. T. Sundari, R. Krishnan, K. N. Prakash, Y. C. Chen, and M. Chavali, J. Nanosci. Nanotechnol. **13**, 1938 (2013).
[48]Z. Hu, G. Wang, Z. Huang, X. Meng, Q. Zhao, and J. Chu, Appl. Phys. A **78**, 757 (2004).
[49]J. Lappalainen, J. Hiltunen, and V. Lantto, J. Eur. Ceram. Soc. **25**, 2273 (2005).
[50]J.-F. Li, Z.-X. Zhu, and F.-P. Lai, J. Phys. Chem. C **114**, 17796 (2010).
[51]J. Tauc, Mater. Res. Bull. **3**, 37 (1968).
[52]R. Ardebili, J. P. Charles, L. Martin, J. Marucchi, and J. C. Manifacier, Mater. Res. Bull. **25**, 1407 (1990).
[53]A. S. Ahmed, S. M. Muhamed, M. L. Singla, S. Tabassum, A. H. Naqvi, and A. Azam, J. Lumin. **131**, 1 (2011).
[54]S. C. Das, R. J. Green, J. Podder, T. Z. Regier, G. S. Chang, and A. Moewes, J. Phys. Chem. C **117**, 12745 (2013).
[55]I. Aulika, V. Zauls, K. Kundzins, M. Kundzins, and S. Katholy, J. Optoelectron. Adv. Mater. **5**, 755 (2003).
[56]D. Bao, X. Yao, N. Wakiya, K. Shinozaki, and N. Mizutani, Appl. Phys. Lett. **79**, 3767 (2001).
[57]M. A. Mohammed, Eng. and Tech. Journal **27**, 1174 (2009).
[58]C. V. Ramana, R. J. Smith, and O. M. Hussain, Phys. Status Solidi A **199**, R4 (2003).
[59]N. Kumar, U. Parihar, R. Kumar, J. Patel, J. Panchal, and N. padha, Am. J. Mater. Sci. **2**, 41 (2012).
[60]R. S. Reddy, A. Sreedhar, A. S. Reddy, and S. Uthanna, Adv. Mater. Lett. **3**, 239 (2012).
[61]K. H. L. Zhang, V. K. Lazarov, T. D. Veal, F. E. Oropeza, C. F. McConville, R. G. Egdell, and A. Walsh, J. Phys. Condens. Matter **23**, 334211 (2011).
[62]G. D. Cody, T. Tiedje, B. Abeles, B. Brooks, and Y. Goldstein, Phys. Rev. Lett. **47**, 1480 (1981).
[63]K. K. Bharathi, M. N. Alam, R. S. Vemuriab, and C. V. Ramana, RSC Adv. **2**, 941 (2012).
[64]E. S. M. Goh, T. P. Chen, C. Q. Sun, and Y. C. Liu, J. Appl. Phys. **107**, 024305 (2010).
[65]H. Gu, D. Bao, S. Wang, D. Gao, A. Kuang, and X. Li, Thin Solid Films **283**, 81 (1996).